arXiv:1105.3226v2 [nucl-th] 9 Sep 2011

Radial and elliptic flow in Pb+Pb collisions at the Large Hadron Collider from viscous hydrodynamics

Chun Shen,[1,*] Ulrich Heinz,[1,†] Pasi Huovinen,[2,‡] and Huichao Song[3,§]

[1] *Department of Physics, The Ohio State University, Columbus, OH 43210-1117, USA*
[2] *Institut für Theoretische Physik, Johann Wolfgang Goethe-Universität, Max-von-Laue-Straße 1, D-60438 Frankfurt am Main, Germany*
[3] *Lawrence Berkeley National Laboratory, 1 Cyclotron Road, Berkeley, CA 94720, USA*

(Dated: February 17, 2022)

A comprehensive viscous hydrodynamic fit of spectra and elliptic flow for charged hadrons and identified pions and protons from Au+Au collisions of all centralities measured at the Relativistic Heavy Ion Collider is performed and used as the basis for predicting the analogous observables for Pb+Pb collisions at the Large Hadron Collider at $\sqrt{s} = 2.76$ and $5.5\,A$ TeV. Comparison with recent measurements of the elliptic flow of charged hadrons by the ALICE experiment shows that the model slightly over-predicts the data if the same (constant) specific shear viscosity η/s is assumed at both collision energies. In spite of differences in our assumptions for the equation of state, the freeze-out temperature, the chemical composition at freeze-out, and the starting time for the hydrodynamic evolution, our results agree remarkably well with those of Luzum [M. Luzum, Phys. Rev. C **83**, 044911 (2011)], indicating robustness of the hydrodynamic model extrapolations. Future measurements of the centrality and transverse momentum dependence of spectra and elliptic flow for identified hadrons predicted here will further test the model and shed light on possible variations of the quark-gluon transport coefficients between RHIC and LHC energies.

PACS numbers: 25.75.-q, 12.38.Mh, 25.75.Ld, 24.10.Nz

I. INTRODUCTION

The first measurement of elliptic flow in Pb+Pb collisions at the Large Hadron Collider (LHC) has just been reported [1]. The elliptic flow coefficient v_2 characterizes the momentum anisotropy of final particle emission in non-central heavy-ion collisions relative to the event-plane, defined by the beam direction and the minor axis of the nuclear overlap region in the collision. It describes the efficiency of the medium generated in the collision to generate from an initial spatial deformation of its density distribution an asymmetry in the final momentum distribution, through interactions of the medium constituents. This efficiency increases with the coupling strength between those constituents and becomes maximal for an infinitely strongly coupled medium. In this limit the mean free path of the constituents becomes as small as allowed by the uncertainty relation [2], and the medium reaches very quickly a state of approximate local thermal equilibrium which allows to describe its evolution with fluid dynamics. For given initial spatial deformation of the collision fireball, ideal fluid dynamics (which assumes zero mean free path) is expected to generate the largest possible elliptic flow [3]. Shear viscosity, a consequence of non-zero mean free paths and limited from below by quantum mechanics [2, 4], will lead to a suppression of v_2 [5, 6].

Compelling evidence for fluid dynamical behavior of the collision fireballs created in ultrarelativistic heavy-ion collisions, with a very small ratio of shear viscosity to entropy density, η/s, has been found in heavy-ion collisions at the Relativistic Heavy Ion Collider (RHIC) [7–10]. The new data from the LHC confirm this picture [1, 11, 12] and agree, at least qualitatively, with hydrodynamic predictions of elliptic flow for Pb+Pb collisions at the LHC [13–19].

The purpose of the present article is to explore how good this agreement is quantitatively, and to what extent the present and future LHC elliptic flow data can tell us novel facts about the transport behavior of hot QCD matter at temperatures that exceed those accessible at RHIC but are within reach at the LHC. Similar to the analyses in [11, 14, 16, 19], but different from recent hybrid model studies in [18, 20], we base our analysis on a purely hydrodynamic approach. While this ignores the fact that the late dilute hadronic stage of the expansion is very dissipative and not well described by fluid dynamics (neither ideal [21] nor viscous [22]), the importance of the hadronic phase for the development of elliptic flow is expected to be much reduced at the LHC relative to RHIC [18, 23]. As in Refs. [11, 16, 19, 20], but different from Refs. [14, 18], we use *viscous* hydrodynamics with a non-zero (but constant, i.e. temperature independent) specific shear viscosity η/s, adjusted to spectra and elliptic flow measurements at RHIC. Our fitted value $\eta/s = 0.20$ (for CGC initial conditions, see below) is 25% larger than that used by Luzum and Romatschke [11, 16] but agrees well with the value for the quark-gluon plasma (QGP) viscosity $(\eta/s)_{\rm QGP}$ recently extracted from RHIC data by using a hybrid viscous hydrodynamic + Boltz-

*Correspond to shen@mps.ohio-state.edu
†Email: heinz@mps.ohio-state.edu
‡Email: huovinen@th.physik.uni-frankfurt.de
§Email: HSong@LBL.gov

mann approach (VISHNU [10, 22]). Calculations with such a hybrid approach are numerically much more demanding than purely hydrodynamic simulations; a generalization of the present analysis using VISHNU will follow soon and should further improve the reliability of the LHC predictions.

II. HYDRODYNAMIC FIT OF RHIC AU+AU DATA

In this work, we employ (2+1)-d viscous hydrodynamics [24] with the lattice QCD based equation of state s95p-PCE [25, 26], which accounts for chemical freeze-out before thermal decoupling at $T_{\rm chem} = 165\,{\rm MeV}$, to simulate the expansion of the collision fireball. From the analysis [10] of charged hadron spectra and elliptic flow in $200\,A\,{\rm GeV}$ Au+Au collisions at RHIC we take over a value of $\eta/s = 0.20$ (corresponding to MC-KLN initial conditions, see below) for the effective specific shear viscosity of the strongly interacting fluid. Using the insights obtained from the systematic parameter study presented in [26], we initialize the hydrodynamic expansion at time $\tau_0 = 0.6\,{\rm fm}/c$ and decouple at $T_{\rm dec} = 120\,{\rm MeV}$ at both RHIC and LHC energies. For Au+Au collisions at RHIC energies these parameters allow for a good global description of the hadron p_T-spectra and differential elliptic flow (see below). Lacking strong theoretical or phenomenological guidance how to adjust their values for Pb+Pb collisions at the LHC, we here decided to keep them unchanged.

At thermalization time τ_0, we assume that the shear stress tensor is given by its Navier-Stokes value $\pi^{\mu\nu} = 2\eta\sigma^{\mu\nu}$ (where $\sigma^{\mu\nu} = \nabla^{\langle\mu}u^{\nu\rangle}$ is the symmetric and traceless velocity shear tensor), and that the initial expansion flow is entirely longitudinal with Bjorken profile $v_z = z/t$ and zero transverse flow velocity. In Milne coordinates (τ, x, y, η) this corresponds to an initial flow 4-velocity $(u^\tau, u^x, u^y, u^\eta) = (1, 0, 0, 0)$. Kinetic freeze-out is implemented by converting the hydrodynamic output to particle spectra with the Cooper-Frye prescription [27] on a decoupling surface of constant temperature $T_{\rm dec}$. We use a quadratic ansatz $\delta f(x,p) \sim p^\mu p^\nu \pi_{\mu\nu}(x)$ [6] for the viscous deviation from local thermal equilibrium of the local phase-space distribution function on the freeze-out surface. Our final hadron spectra include decay products from strong decays of all particles and resonances up to 2 GeV mass [28], using the resonance decay program from the AZHYDRO package.[1]

For the initial density profile we here use a Monte-Carlo version [29, 30] of the Kharzeev-Levin-Nardi [31] model (MC-KLN).[2] The specific implementation used in this work is described in [18, 32]. The model gives for each event the gluon density distribution in the transverse plane. We assume it to thermalize by time τ_0, and convert the gluon density into entropy density [21]. Over one million Monte Carlo events are re-centered to the beam axis and rotated in the transverse plane such that their minor axis aligns with the impact parameter (i.e. their "participant plane" coincides with the reaction plane). After sorting them into collision centrality bins according to their number $N_{\rm part}$ of participating ("wounded") nucleons, we average them to obtain a smooth average initial entropy density which is then converted to energy density using the equation of state. Using this smooth energy density as weight, we compute the initial eccentricity $\bar{\varepsilon} = \frac{\langle y^2 - x^2\rangle}{\langle y^2 + x^2\rangle}$ and overlap area $S = \pi\sqrt{\langle x^2\rangle\langle y^2\rangle}$ of the reaction zone; these represent the corresponding mean values of events in this centrality class.[3]

The KLN model involves a couple of parameters that need to be adjusted to obtain the correct final charged hadron multiplicity $dN_{\rm ch}/d\eta$ in central Au+Au collisions at RHIC. In [32] this adjustment was performed for ideal fluid dynamics (which conserves entropy) coupled to a hadron cascade. The model then correctly predicts the charged hadron multiplicities at all other collision centralities. In our viscous hydrodynamic model, viscous heating produces additional entropy, leading to somewhat larger final multiplicities. We thus perform an iterative renormalization of the initial entropy density profile until the measured charged hadron multiplicity in the 0−5% most central $200\,A\,{\rm GeV}$ Au+Au collisions at RHIC is once again reproduced. The lower panel of Fig. 1 shows that, after this renormalization, the model again correctly describes the measured [34] centrality dependence of charged hadron production. The centrality dependence of viscous entropy production (which is relatively larger in peripheral than in central collisions [24]) is (at least at RHIC energies) sufficiently weak to not destroy the agreement of the model with experimental observations.

The ability of the MC-KLN model to describe the centrality dependence of charged hadron production without additional parameters is the main reason for choosing it over the MC-Glauber model as our basis for extrapolation from RHIC to LHC energies. It was recently shown [35] that this centrality dependence is robust against running coupling corrections [36–38] in the Balitsky-Kovchegov evolution (on which the KLN model is based) which were found to hardly affect its shape. They do, however, modify the collision energy dependence of particle production, with the LHC Pb+Pb data

[1] AZHYDRO is available at the URL http://www.physics.ohio-state.edu/~froderma/.

[2] The Monte Carlo code is available at URL http://www.aiu.ac.jp/~ynara/mckln/.

[3] Note that about 10% larger overlap areas are obtained when using the entropy density as weight [10, 18], whereas for all but the most central collisions the eccentricities of the energy and entropy densities are nearly identical [33].

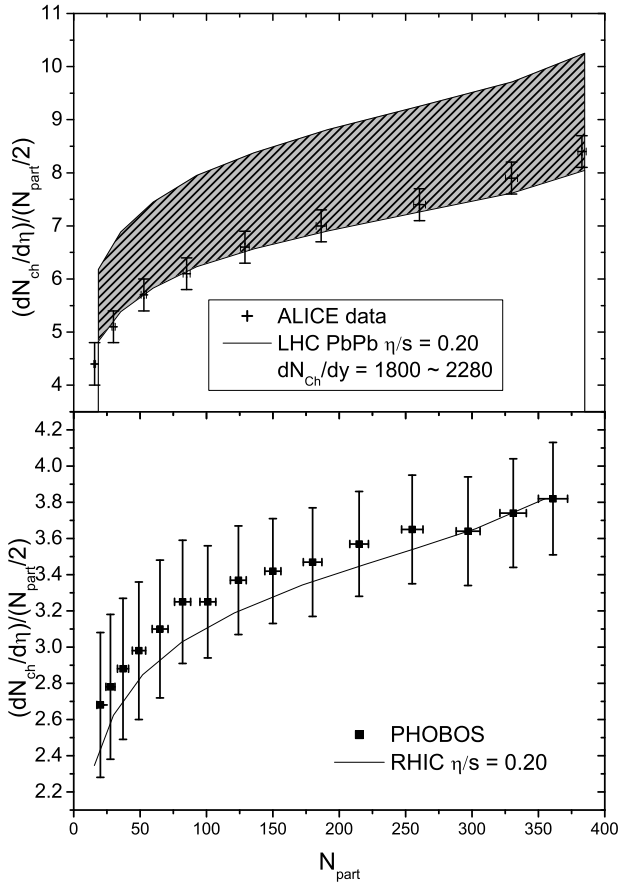


FIG. 1: Centrality dependence of the charged hadron multiplicity per unit pseudo-rapidity, $dN_{\rm ch}/d\eta/(N_{\rm part}/2)$ as a function of $N_{\rm part}$, in 200 A GeV Au+Au collisions at RHIC (bottom panel) and in $(2.76-5.5)$ A TeV Pb+Pb collisions at the LHC (top panel). Experimental data are from the PHOBOS Collaboration [34] for Au+Au collisions at $\sqrt{s}=200\,A$ GeV, and from the ALICE Collaboration [39] for Pb+Pb collisions at $\sqrt{s}=2.76\,A$ TeV. The lines are from the MC-KLN model (see text). For Au+Au at RHIC the MC-KLN model was normalized to the measured multiplicity in the 0-5% centrality bin; at the LHC, the lines bounding the shaded region were normalized to $dN_{\rm ch}/d\eta=1548$ and 1972 (or $dN_{\rm ch}/dy=1800$ and 2280) at 0-5% centrality, respectively.

being better described if running coupling corrections are included [39]. Our version of the MC-KLN model does not include running coupling corrections,[4] and we must normalize the initial entropy density profile for Pb+Pb collisions at the LHC separately from Au+Au collisions at RHIC. Without such an independent renormalization, we overpredict the measured charged multiplicity from central 2.76 A TeV Pb+Pb collisions [39, 40] by about 10%.

After renormalization we obtain the solid lines bounding the shaded region in the upper panel of Fig. 1, with the lower (upper) bound corresponding to Pb+Pb collisions at 2.76 (5.5) A GeV, respectively. The data in that panel are from the ALICE Collaboration for Pb+Pb at 2.76 A GeV [39, 40]. (For 5.5 A GeV Pb+Pb collisions we assumed $dN_{\rm ch}/dy=2280$ (corresponding to $dN_{\rm ch}/d\eta=1972$), based on an extrapolation of Fig. 3 in Ref. [40].) One sees that, even without running coupling corrections, but including viscous entropy production, the MC-KLN model does a good job in describing the measured centrality dependence of charged hadron production in Pb+Pb collisions at the LHC. This gives hope that the successful description of the centrality dependence of hadron spectra and elliptic flow at RHIC energies (see below and [10]) translates into a reliable prediction of the corresponding centrality dependences in Pb+Pb collisions at the LHC.

Figures 2 and 3 establish our baseline for the extrapolation to LHC energies. In Fig. 2 we show our purely hydrodynamic fit (obtained with parameters τ_0, η/s, $T_{\rm chem}$, and $T_{\rm dec}$ set as described above[5]) of the hadron spectra measured in 200 A GeV Au+Au collisions at RHIC. Fig. 2a shows the mid-rapidity transverse momentum spectra per unit pseudo-rapidity for unidentified charged hadrons from the STAR [41] and PHENIX [42] experiments compared with the hydrodynamical model. Figs. 2b,c show a similar comparison for the p_T-spectra per unit rapidity of identified pions and protons from STAR [43, 44] and PHENIX [45]. In the experimental spectra, protons from weak decays were removed; STAR quotes a large systematic error associated with this feeddown correction, and within that large error band the two data sets agree with each other, even if the central values of the STAR proton data appear to be up to 50% higher than PHENIX data. Our results agree well with the STAR protons for $p_T > 0.6\,{\rm GeV}/c$ but overpredict the PHENIX protons by up to a factor 2.

Figure 3 shows the hydrodynamically calculated differential elliptic flow for unidentified charged hadrons in comparison with STAR $v_2\{4\}(p_T)$ data [46, 47], for four centrality classes ranging from semi-central to mid-peripheral collisions (10−50% centrality). With $\eta/s=0.20$, viscous hydrodynamics gives an excellent description of the STAR $v_2\{4\}$ data, even up to 3 GeV/c in transverse momentum (i.e. beyond the p_T range where the hydrodynamic description is expected to begin to

[4] The `rcBK` code in [35] includes running coupling corrections but it has not been renormalized to take into account viscous entropy production at RHIC energies.

[5] Note that our value $\tau_0=0.6\,{\rm fm}/c$ is 45% smaller than the value of $1.05\,{\rm fm}/c$ used for $\eta/s=0.2$ in the `VISHNU` simulations in [10]. The earlier evolution of hydrodynamic transverse flow arising from this smaller τ_0 value compensates for the lack of a highly dissipative hadronic phase in the purely hydrodynamic approach. Hadronic dissipation leads to a significant broadening in particular of the proton p_T-spectra during the hadronic stage which (given the constraints from the elliptic flow data which prohibit us from simply lowering $T_{\rm dec}$) viscous hydrodynamics with temperature-independent $\eta/s=0.2$ cannot replicate.

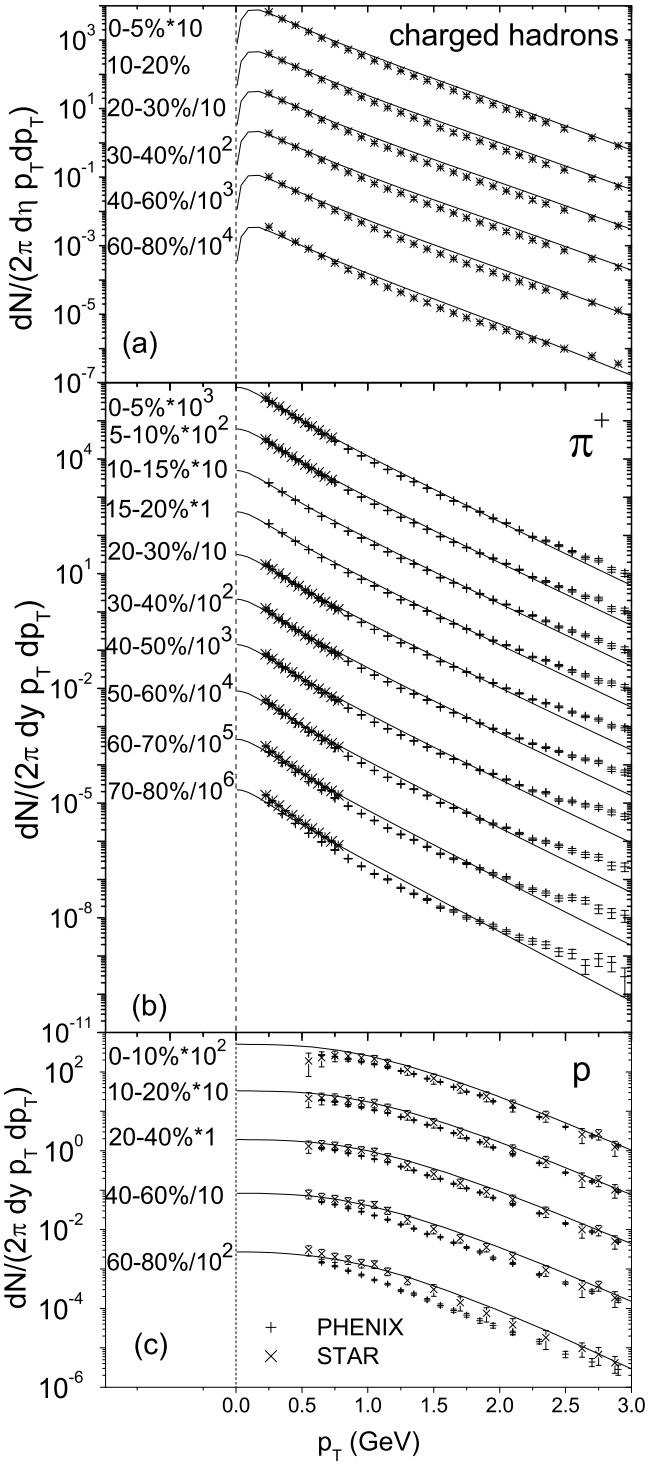


FIG. 2: p_T-spectra of all charged hadrons (a), positive pions (b) and protons (c) for 200 A GeV Au+Au collisions of different centralities as indicated. The symbols show data from the STAR ([41, 43, 44], ×) and PHENIX ([42, 45], +) experiments. The lines are results from the viscous hydrodynamic model for constant $\eta/s = 0.20$ and MC-KLN initial conditions (see text for other model parameters).

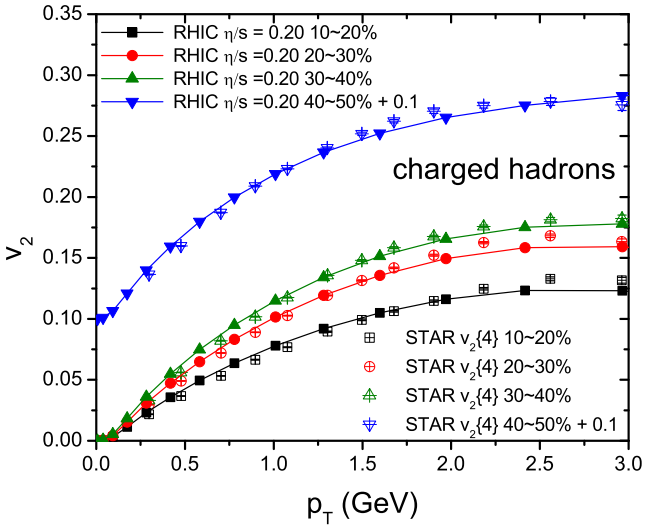


FIG. 3: (Color online) Differential elliptic flow $v_2(p_T)$ for charged hadrons from 200 A GeV Au+Au collisions of different centralities as indicated. Open symbols are experimental data from the STAR experiment for $v_2\{4\}(p_T)$ [46, 47], lines with filled symbols of the same shape are the corresponding hydrodynamic fits with the same model as in Fig. 1. For the 40−50% centrality bin data and theory are vertically offset by 0.1 for better visibility.

break down, due to the increasing influence of hard production processes and large uncertainties in the viscous correction δf to the local phase-space distribution at kinetic freeze-out [48]). Looking more carefully one sees that our model slightly overestimates the elliptic flow at low $p_T < 1$ GeV while underestimating it in the high-p_T region, $p_T > 2$ GeV.

In [26] we noted a tension in trying to simultaneously fit within a purely viscous hydrodynamic approach the proton p_T-spectra and the charged hadron differential elliptic $v_2^{\rm ch}\{2\}(p_T)$ when using EOS `s95p-PCE`. Even a temperature dependent $\eta/s(T)$ that has a larger shear viscosity in the hadronic phase could not resolve this tension: in [48] two of us found that the RHIC Au+Au hadron spectra are insensitive to a temperature-dependent increase of the shear viscosity in the hadron gas phase, as was previously seen in [49]. Figs. 2 and 3 demonstrate that this problem is largely resolved when using the $v_2\{4\}(p_T)$ data (Fig. 3) instead of $v_2\{2\}$ (see Fig. 8 further below): We obtain an excellent description of the differential elliptic flow, together with an acceptable description (within large experimental uncertainties) of the p_T spectra.

Overall, the viscous fluid dynamic description of the hadron spectra and charged hadron elliptic flow $v_2(p_T)$ shown here is of similar quality as the hybrid model description with `VISHNU` presented in [10]. Since purely hydrodynamic simulations are numerically much less costly than calculations with `VISHNU`, we will now use them to generate a broad range of predictions for soft hadron production in Pb+Pb collisions at the LHC.

III. PREDICTIONS FOR PB+PB COLLISIONS AT THE LHC

As discussed above, the extrapolation from RHIC to LHC is done keeping τ_0, $T_{\rm chem}$, $T_{\rm dec}$ and η/s fixed. When comparing the resulting viscous hydrodynamic predictions with experimental data from the recently started LHC heavy-ion collision program, we will search for indications from experiment that would motivate changing these parameters. First results for p_T-spectra [50] as well as both the p_T-differential and p_T-integrated elliptic flow of unidentified charged hadrons [1] have already been published and will be compared with the theoretical predictions below. Additional experimental information on spectra and elliptic flow of identified hadrons will become available soon; the relevant hydrodynamic predictions are presented in this section.

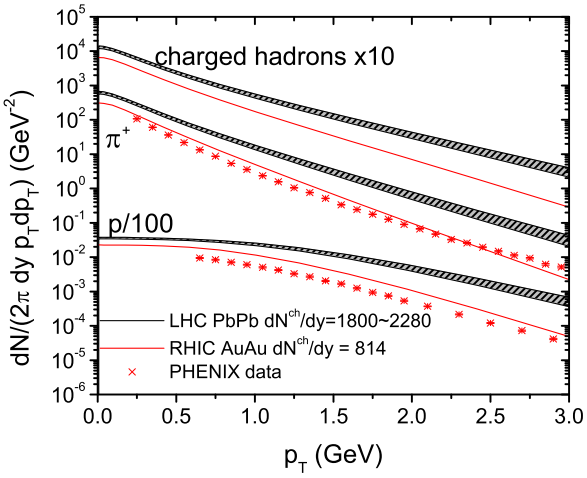


FIG. 4: (Color online) p_T-spectra of all charged hadrons, positive pions, and protons for minimum bias 200 A GeV Au+Au (thin red lines and data points) and (2.76−5.5) A TeV Pb+Pb collisions (black lines with shaded area). The RHIC data are from the PHENIX experiment [45]. The shaded bands for the LHC predictions are limited at the bottom (top) by lines for $\sqrt{s}=2.76$ (5.5) A TeV, corresponding to $dN_{\rm ch}/dy=1800$ (2280) ($dN_{\rm ch}/d\eta=1548$ (1972)). The calculations assume the same constant $\eta/s=0.2$ at all shown collision energies.

In Fig. 4 we show the transverse momentum spectra for all charged hadrons, as well as for identified pions and protons, for minimum bias collisions of Au+Au at RHIC and Pb+Pb at the LHC.[6] For RHIC we compare with data from the PHENIX Collaboration [45]. The upper and lower bounds of the shaded areas are predictions for minimum bias Pb+Pb collisions at collision energies of 5.5 and 2.76 TeV per nucleon pair, respectively. The LHC spectra are visibly flatter than at RHIC energies, reflecting stronger radial flow. For central collisions (0−5% centrality), the fireball lifetime increases from Au+Au at RHIC to Pb+Pb at LHC by about 19% and 24%, respectively, for 2.76 and 5.5 A TeV collision energy; for peripheral collisions at 70−80% centrality, the corresponding lifetime increases are even larger (34% and 41%, respectively). The average radial flow velocity increases in central collisions (0−5% centrality) by 5 and 7%, respectively, and in peripheral collisions (70−80% centrality) by 9 and 11%.

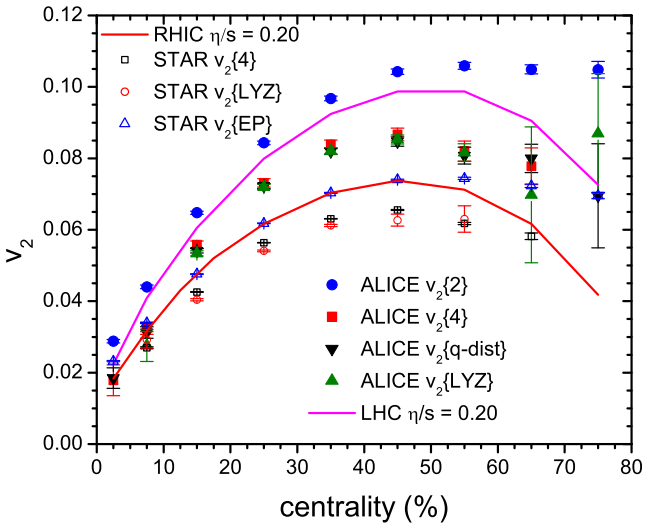


FIG. 5: (Color online) p_T-integrated elliptic flow of charged hadrons for 200 A GeV Au+Au collisions at RHIC (open symbols are STAR data [46, 47], the lower red line is the result from viscous hydrodynamics) and for 2.76 A TeV Pb+Pb collisions at the LHC (filled symbols are ALICE data [1], the upper magenta line shows the viscous hydrodynamic prediction). In both experiment and theory the differential elliptic flow $v_2(p_T)$ (see Figs. 3 and 7) was integrated over the range $0.15\,{\rm GeV}/c<p_T<2\,{\rm GeV}/c$ for Au+Au at RHIC and over $p_T>0.2\,{\rm GeV}/c$ for Pb+Pb at the LHC.

Figure 5 shows the integrated charged hadron elliptic flow v_2 as a function of collision centrality for Au+Au collisions at RHIC and Pb+Pb collisions at the LHC. At RHIC energy, our results (lower red line) overestimates the STAR $v_2\{4\}$ data by about 11% in mid-central collisions, but agrees nicely with $v_2\{{\rm EP}\}$ except for the most peripheral collisions.[7] At first sight the overprediction of the p_T-integrated $v_2\{4\}$ at RHIC is surprising, given

[6] To simulate minimum bias collisions, we compute the spectra for the centrality classes shown in Figs. 2(b) and 6 and average them. Any additional observables, such as the minimum bias elliptic flow in Fig. 8 below, are calculated from these minimum bias spectra.

[7] In very peripheral collisions, the fireball lifetime decreases dramatically, cutting short the buildup of anisotropic hydrodynamic flow and thereby prohibiting v_2 from saturating. In addition, viscous effects are stronger in the small fireballs created in peripheral collisions than in the larger central collision fireballs. Both effects together cause the theoretical v_2 values to decrease sharply at large collision centralities, in apparent conflict with

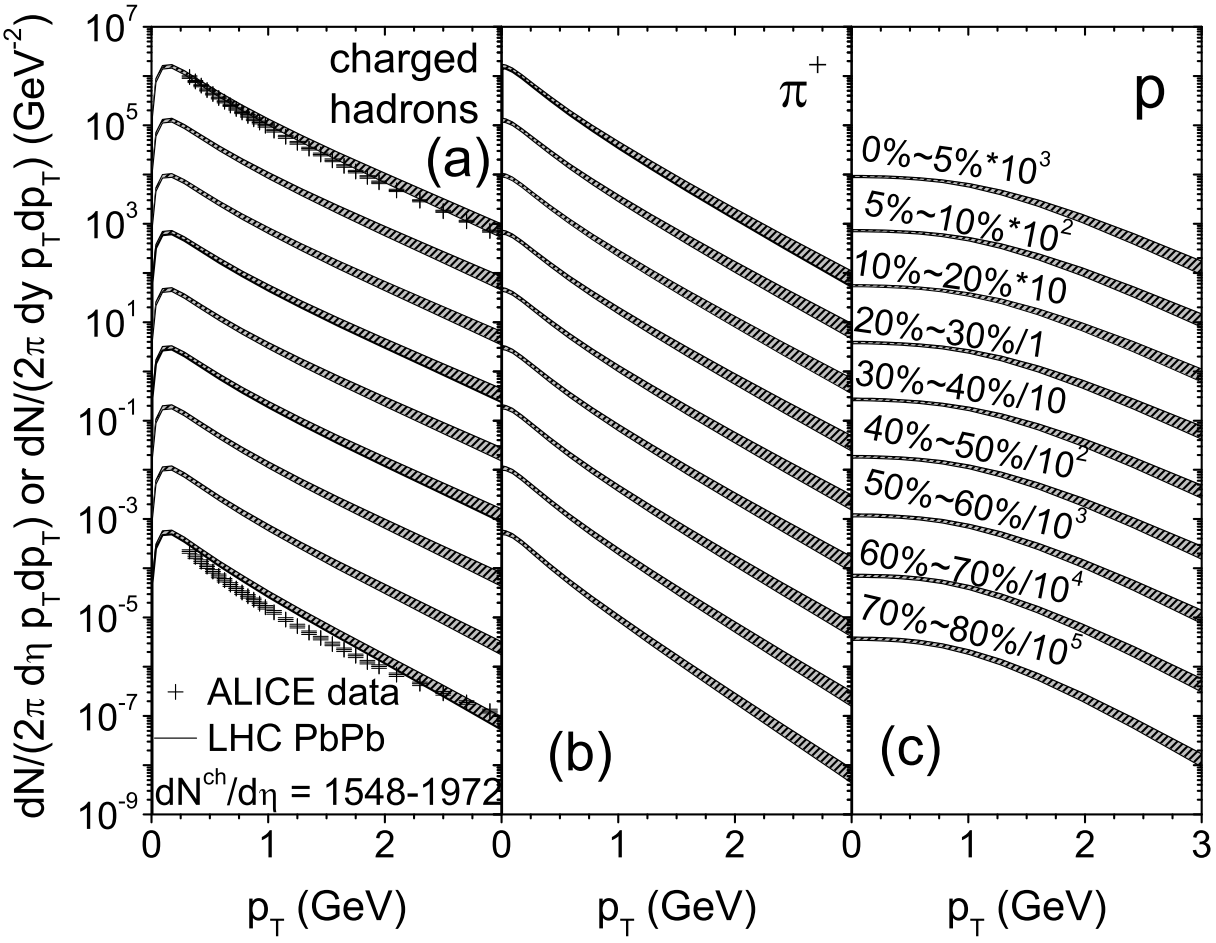


FIG. 6: p_T-spectra per unit pseudorapidity for charged hadrons (a) and per unit rapidity for pions (b) and protons (c) for Pb+Pb collisions at the LHC. The lower and upper end of the shaded bands represent viscous hydrodynamic predictions for $\sqrt{s} = 2.76$ and 5.5 A TeV (corresponding to $dN_{\rm ch}/d\eta = 1548$ and 1972, or $dN_{\rm ch}/dy = 1800$ and 2280), respectively. Experimental data in panel (a) are from the ALICE experiment [50].

the excellent description of the differential elliptic flow $v_2\{4\}(p_T)$ shown in Fig. 3. The apparent paradox is resolved by observing that the hydrodnamically computed charged hadron p_T-spectra shown in Fig. 2 are somewhat harder than measured, thereby giving too much weight in the p_T-integral to the range $0.75 < p_T < 2\,{\rm GeV}/c$ where $v_2\{4\}(p_T)$ is large.[8]

At LHC energy ($\sqrt{s} = 2.76\,A\,{\rm TeV}$) our integrated v_2 lies between $v_2\{2\}$ and $v_2\{4\}$ values measured by the ALICE Collaboration [1]. Again, we overpredict the p_T-integrated $v_2\{4\}$ by about 10−15%. We note that from RHIC to LHC the hydrodynamically computed integrated v_2 in mid-central to mid-peripheral collisions increases by about 30%, in agreement with the experimental observations. This is due to reduced viscous suppression effects in the larger and denser fireballs created at the LHC and a longer fireball lifetime which allows the momentum flow anisotropy to approach saturation more closely than at lower energies [23, 53]. In very peripheral collisions, even at LHC energies such a saturation of v_2 does not happen; this is the reason why in Fig. 5 the integrated v_2 is seen to decrease at large collision centralities, both at RHIC and LHC.

In Fig. 6 we present hadron transverse momentum spectra for Pb+Pb collisions at LHC energies, for a range of collision centralities. In panel (a) we compare the hydrodynamic predictions with first data from the ALICE experiment [50]. Overall, the theoretical descrip-

the experimental data. The experimental $v_2\{2\}$ and $v_2\{{\rm EP}\}$ measurements are, however, contaminated by non-flow effects, in particular in very peripheral collisions. Once non-flow effects are corrected for [51], the experimental v_2 values decrease at large collision centralities much in the same way as predicted by hydrodynamics.

[8] The agreement with the $v_2\{{\rm EP}\}$ data is fortuitous and should, in fact, not happen since the measured $v_2\{{\rm EP}\}$ includes a positive contribution from event-by-event v_2 fluctuations [52] while our hydrodynamic calculation yields the average elliptic flow $\langle v_2 \rangle$ which is smaller.

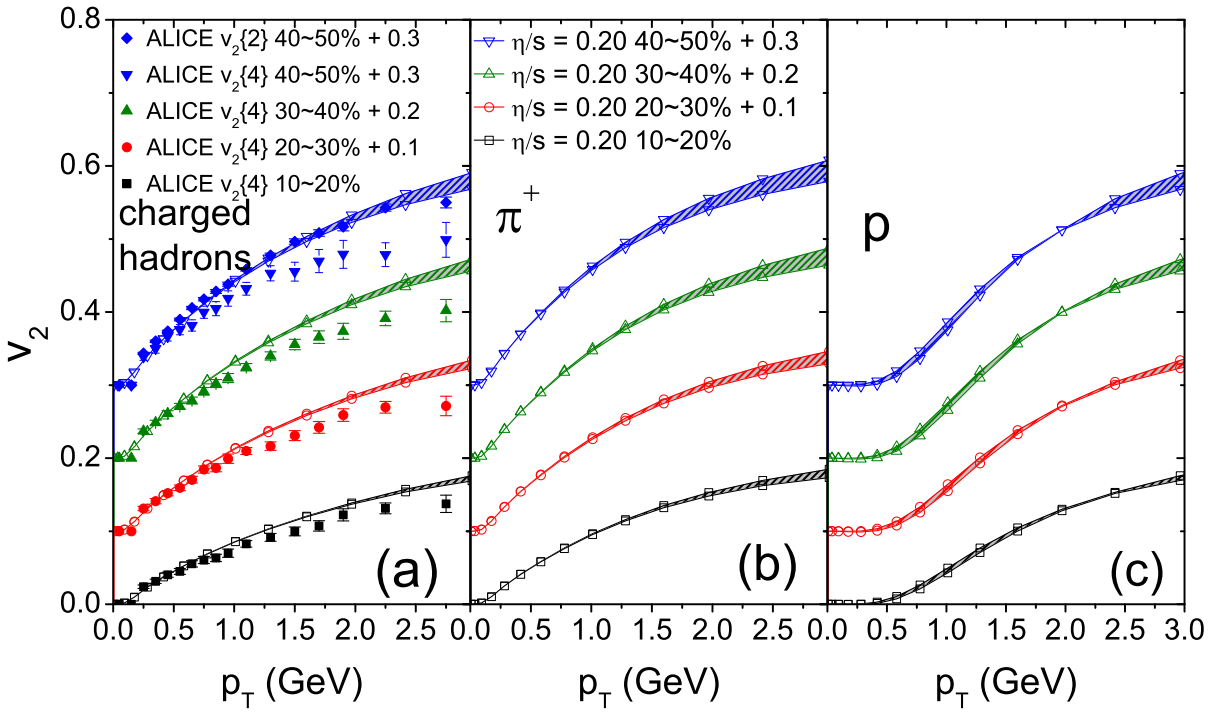


FIG. 7: (Color online) Differential elliptic flow $v_2(p_T)$ for unidentified charged hadrons (a) and identified pions (b) and protons (c), for Pb+Pb collisions of different centralities at the LHC. Experimental data for charged hadron $v_2(p_T)$, denoted by solid symbols, are from the ALICE experiment [1]; they should be compared with theoretical lines carrying open symbols of the same shape and color. The shaded bands show the variation of the hydrodynamic predictions with collision energy between $\sqrt{s} = 2.76$ and 5.5 TeV (corresponding to $dN_{\rm ch}/dy = 1800$ and 2280, respectively). The lines corresponding to the lower collision energy ($\sqrt{s} = 2.76$ TeV) define the lower end of the shaded regions at $p_T = 3\,{\rm GeV}/c$.

tion of these experimental data is of similar quality as for Au+Au collisions at RHIC (see Fig. 2). In the most central collisions, the hydrodynamical model describes the charged hadron spectrum somewhat better than at RHIC, whereas in the very peripheral collisions the hydrodynamic spectra are too flat, presumably due to large viscous shear pressure effects. Future comparison with the measured spectra at other collision centralities and for identified hadrons, shown here in panels (b) and (c) as predictions, should shed further light on the origin of the discrepancy in peripheral collisions.

Figure 7a shows a comparison of the hydrodynamically generated differential $v_2^{\rm ch}(p_T)$ for charged hadrons with the ALICE $v_2\{4\}$ data [1], for four different collision centralities. For the most peripheral of these, we also show the measured $v_2\{2\}$ for comparison. The hydrodynamic predictions agree nicely with the data at low $p_T < 1\,{\rm GeV}/c$, but overshoot the experimental values by 10−20% at larger p_T, especially in the more peripheral bins. In the 40−50% centrality bin, the theoretical prediction happens to agree nicely with $v_2\{2\}(p_T)$ even though the latter should be shifted upward by flow fluctuations that are not included in the theoretical calculation. We note that the theoretical overshoot is less severe in the VISHNU hybrid model (see Fig. 3 in [20]) than in the purely hydrodynamic simulations shown here. This suggests that the excess of $v_2(p_T)$ over the measured values at $p_T > 1\,{\rm GeV}/c$ in Fig. 7a may be caused by an inadequate description of the late hadronic stage and its freeze-out.

We can summarize Figs. 2a, 3, 5, 6, and 7a by observing that the hydrodynamic model overpredicts the p_T-integrated charged hadron v_2 by 10−15% at both RHIC and LHC, but for different reasons: at RHIC the differential elliptic flow $v_{2,{\rm ch}}(p_T)$ is correctly reproduced while the inverse slope of the theoretical p_T-spectra is slightly too large, while the LHC p_T-spectra are described a bit better (at least in the most central collisions where published data are available) but the slope of $v_{2,{\rm ch}}(p_T)$ at the LHC is slightly overpredicted.

Panels (b) and (c) of Fig. 7 give predictions for the differential $v_2(p_T)$ of identified pions and protons. Please note the different shape of the proton $v_2(p_T)$ from that of the pions at low p_T: radial flow pushes the proton elliptic flow to larger values of p_T. Comparing the curves for $\sqrt{s} = 2.76$ and 5.5 A TeV, we see that this "radial push" of the proton v_2 increases with collision energy, so for higher $\sqrt{s}$ the rise of $v_2(p_T)$ is shifted to larger transverse momenta, while at fixed $p_T < 1.5\,{\rm GeV}/c$ the proton elliptic flow *decreases* with increasing collision energy. This happens only for heavy hadrons but not for the much lighter pions (see panel (b)).

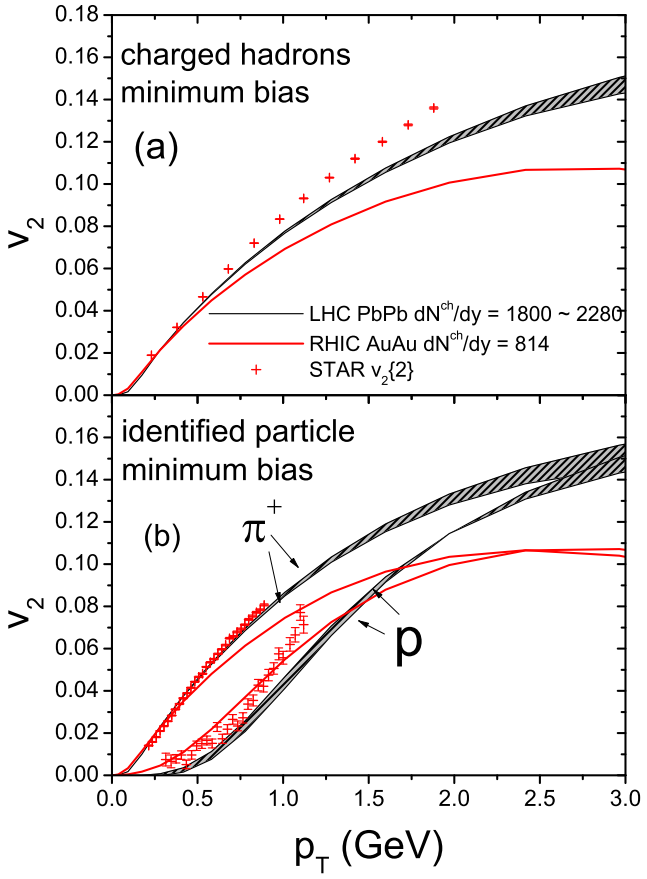


FIG. 8: (Color online) Differential elliptic flow $v_2(p_T)$ for all charged hadrons (a) and identified pions and protons (b), for minimum bias 200 A GeV Au+Au collisions at RHIC and (2.76−5.5) A TeV Pb+Pb collisions at the LHC. Experimental data for $v_2\{2\}$ from Au+Au collisions at RHIC are from the STAR experiment [54]. Solid lines are viscous hydrodynamic results for 200 A GeV Au+Au collisions with the same hydrodynamic parameters as in Figs. 1-4; note their disagreement with the $v_2\{2\}$ data shown here (in contrast to their excellent agreement with $v_2\{4\}$ data shown in Fig. 3). The shaded bands are LHC predictions and show the variation of the theoretical expectations for Pb+Pb collisions at collision energies ranging from $\sqrt{s}=2.76$ to 5.5 A TeV (corresponding to $dN_{\rm ch}/dy=1800$ and 2280, respectively). As in Fig. 7, the lines defining the lower end of the shaded region at $p_T=3$ GeV/c correspond to the lower LHC energy $\sqrt{s}=2.76$ A TeV.

In Figs. 8 and 9 we pursue this theme further, by directly comparing the differential elliptic flows at RHIC and LHC energies. In Fig. 8 we show results for minimum bias collisions; the RHIC predictions are compared with available data from STAR [54]. We see that at low p_T, the elliptic flow for unidentified charged hadrons (which are strongly pion dominated) and for identified pions increases from RHIC to LHC whereas the opposite is true for protons. At higher p_T ($p_T > 1.5$ GeV/c), on the other hand, $v_2(p_T)$ increases for *both* pions and protons as we increase the collision energy. Fig. 9 shows this for a few more hadron species, for the 10−20% and 40−50% centrality bins: the heavier the hadron, the stronger a push of v_2 towards higher p_T is observed. At sufficiently large p_T, $v_2(p_T)$ is larger at LHC than at RHIC for all particle species, but at low p_T this holds only for pions whereas all heavier hadrons show a decrease of $v_2(p_T)$ from RHIC to LHC at fixed p_T. As the hadron rest mass grows, the crossing point where the decrease of v_2 at fixed p_T with rising collision energy turns into an increase shifts to larger p_T values. In view of Fig. 9, the experimental observation [1] that for unidentified charged hadrons $v_2^{\rm ch}(p_T)$ hardly changes at all from RHIC to LHC appears accidental:[9] The increase of $v_2(p_T)$ at fixed p_T for pions is balanced by a corresponding decrease for all heavier hadrons leaving, as it happens, no visible net effect once all charged hadrons are lumped together.

In Refs. [10] it was argued that a robust method for extracting the QGP shear viscosity is to fit the collision centrality dependence of the eccentricity-scaled charged hadron elliptic flow $v_2^{\rm ch}/\bar{\varepsilon}$ with a viscous hydrodynamic + hadron cascade hybrid code. In that study it was found that, at fixed collision energy,[10] plotting $v_2^{\rm ch}/\bar{\varepsilon}$ against the charged hadron multiplicity density per unit overlap area, $(1/S)(dN_{\rm ch}/dy)$, yields "universal" curves that depend only on the QGP shear viscosity but not on the model for the initial energy density distribution (in particular its eccentricity). In Fig. 10 we show such a plot for 200 A GeV Au+Au collisions at RHIC together with Pb+Pb collisions at two LHC energies. The four panels show this scaling in terms of distributions in pseudorapidity (η, left column) or rapidity (y, right column), and also compare it for our default choice of using the initial *energy* density as weight for the calculation of the average eccentricity $\bar{\varepsilon}$ and overlap area S (top row) with what one obtains by evaluating these quantities with the initial *entropy* density instead (as is done in Refs. [10, 18]) (bottom row). We see that, independent of these choices of representation, the universality of $v_2^{\rm ch}/\bar{\varepsilon}$ vs. $(1/S)(dN_{\rm ch}/dy)$ or $(1/S)(dN_{\rm ch}/d\eta)$ does not carry over to different collision energies (at least not for the purely hydrodynamic simulations studied in the present work): At the same multiplicity density $(1/S)(dN_{\rm ch}/dy)$ or $(1/S)(dN_{\rm ch}/d\eta)$, more peripheral higher energy collisions produce less elliptic flow per initial eccentricity than more central lower energy collisions. At fixed $\eta/s=0.2$, the difference between 200 A GeV Au+Au and

[9] Contrary to the claim made in [12], the observation that the ratio between $v_2^{\rm ch}(p_T)$ measured at LHC and at RHIC is approximately independent of p_T cannot be directly used to conclude that $(\eta/s)_{\rm QGP}$ does not change from RHIC to LHC. If that argument were correct, this ratio should be independent of p_T not only for the sum of all charged hadrons, but also for each identified hadron species separately. Our hydrodynamic calculations show that the latter does not hold even if η/s remains unchanged from RHIC to LHC.

[10] We recently checked that this multiplicity scaling carries over to other collision systems such as Cu+Cu *at the same collision energy* [55].

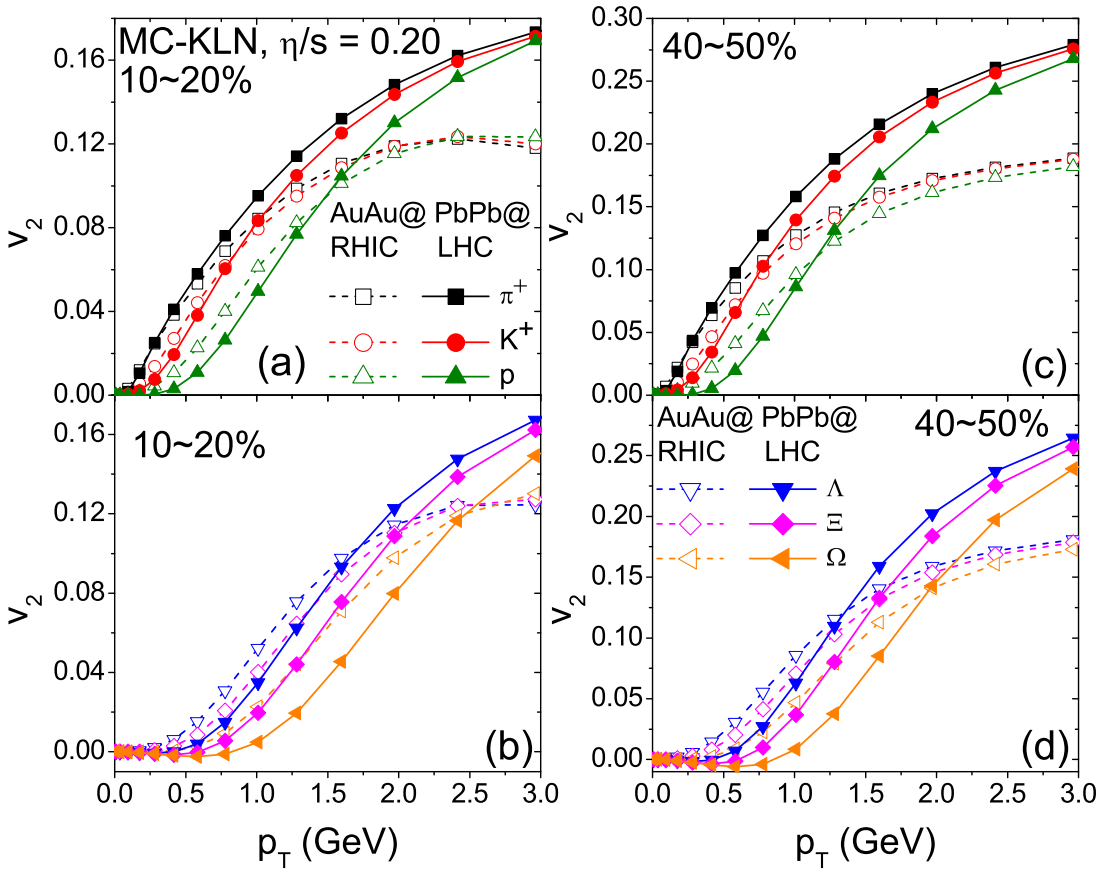


FIG. 9: (Color online) Comparison of the differential elliptic flow $v_2(p_T)$ for 200 A GeV Au+Au collisions at RHIC (dashed lines) and 2.76 A TeV Pb+Pb collisions at the LHC (solid lines), at 10%−20% (a,b) and 40%−50% (c,d) centrality, for a variety of different hadron species. Note the slightly negative elliptic flow for the heavy Ω hyperons at low p_T.

2.76 A TeV Pb+Pb collisions (red circles vs. green upward triangles in Fig. 10) is as large as the difference between $\eta/s = 0.16$ and $\eta/s = 0.20$ for Au+Au collisions at fixed $\sqrt{s} = 200$ A GeV (red circles vs. black squares).

We note that the tendency in Fig. 10 of higher energy collisions producing less $v_2^{\rm ch}/\bar{\varepsilon}$ at fixed $(1/S)(dN_{\rm ch}/dy)$ than lower energy ones contradicts the opposite tendency observed by Hirano *et al.* in Fig. 3 of Ref. [18] where an ideal hydro + hadron cascade hybrid code was employed.[11] The authors of [18] presented strong arguments that their observation of larger $v_2^{\rm ch}/\bar{\varepsilon}$ at fixed $(1/S)(dN_{\rm ch}/d\eta)$ in higher energy collisions is not related to their use of a hadron cascade for describing the late hadronic stage. Our opposite finding, on the other hand, is supported by the earlier purely hydrodynamic scaling studies presented in the last two works of [24] whose authors came to the same conclusion as we do here. At present this discrepancy remains unresolved; we suspect, however, that the origin of the difference between our work and that of Hirano *et al.* could be in their use of a more realistic (3+1)-dimensional hydrodynamic evolution [56], although in the earlier ideal fluid hydrodynamical studies at the full RHIC energy, the differences between boost invariant and non-boost invariant results were small [3, 57]. Possible consequences of the violation of boost-invariance in RHIC and LHC heavy-ion collisions are presently being studied [55].

Before moving on, let us comment on the different shape at the high-multiplicity end of the curves shown in Fig. 10 when using entropy instead of energy density as the weight for calculating the initial eccentricity $\bar{\varepsilon}$ overlap area S: It is caused by the different centrality dependence of the energy and entropy density weighted eccentricities in near-central collisions observed in Ref. [33] whose authors showed that in the most central collisions (where $\bar{\varepsilon}$ is dominated by event-by-event shape fluctuations) the entropy-weighted participant eccentricity decreases faster with decreasing impact parameter than the energy-weighted one.

[11] The careful reader will notice that for 200 A GeV Au+Au collisions, our maximal values for $(1/S)(dN_{\rm ch}/d\eta)$ in Fig. 10b are significantly larger than those shown in Fig. 3 of Ref. [18]. This is due to a lower normalization of the initial entropy density in [18], corresponding to $dN_{\rm ch}/d\eta \sim 600$ instead of our $dN_{\rm ch}/d\eta \sim 700$ in central Au+Au collisions (T. Hirano, private communication).

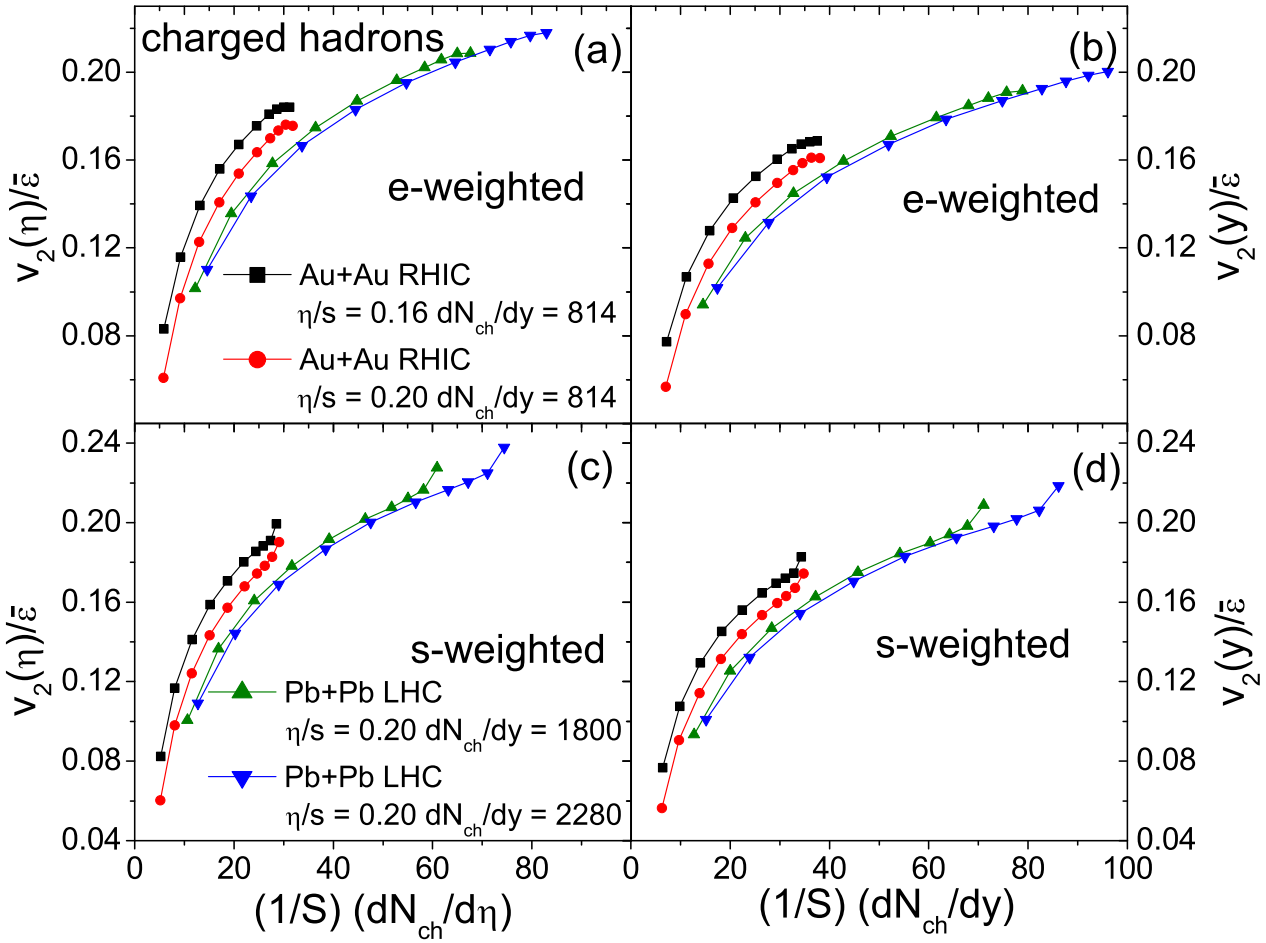


FIG. 10: (Color online) Eccentricity-scaled elliptic flow $v_2/\bar{\varepsilon}$ as function of the charged hadron multiplicity density per unit overlap area S from viscous hydrodynamic calculations at $\sqrt{s}=0.2$, 2.76, and 5.5 A TeV (corresponding to $dN_{\rm ch}/dy=814$ (Au+Au), 1800 and 2280 (Pb+Pb), respectively). Each line corresponds to one collision system at fixed collision energy but different collision centralities (from right to left, the symbols correspond to 0-5%, 5-10%, 10-15%, 15-20%, 20-30%, 30-40%, 40-50%, 50-60%, 60-70% and 70-80% centrality). The four panels show $v_2(\eta)/\bar{\varepsilon}$ vs. $(1/S)(dN_{\rm ch}/d\eta)$ (where η is pseudorapidity) (a,c) and $v_2(y)/\bar{\varepsilon}$ vs. $(1/S)(dN_{\rm ch}/dy)$ (where y is rapidity) (b,d), with $\bar{\varepsilon}$ and S evaluated with the participant-plane averaged energy density $\bar{e}(\boldsymbol{r}_\perp,\tau_0)$ as weight function (a,b) (default option, see Sec. II) or (for comparison with other work) with the corresponding entropy density $\bar{s}(\boldsymbol{r}_\perp,\tau_0)$ as weight (c,d). The RHIC curves for $\eta/s=0.16$ (black squares) illustrate the effect of changing the value of the specific shear viscosity by 0.04. The LHC calculations are done for $\eta/s=0.20$ as obtained from the hydrodynamic fit to RHIC data.

IV. TEMPERATURE DEPENDENT $\eta/s(T)$

Shear viscosity is known to suppress the buildup of elliptic flow. Naively, the systematic overprediction of $v_2\{4\}(p_T)$ in Pb+Pb collisions at the LHC seen in Fig. 7a, together with the excellent description of the same quantity in Au+Au collisions at RHIC seen in Fig. 3, thus suggests that the fireball liquid formed in LHC collisions might be slightly more viscous (i.e. possess larger average η/s) than at RHIC energies [20, 49]. In this section we present some results using a temperature dependent specific shear viscosity, $(\frac{\eta}{s})(T)$, that were motivated by such considerations.

Figure 11 illustrates the following three trial functions explored in this section:

$$\left(\frac{\eta}{s}\right)_1 = 0.2 + 0.3\,\frac{T-T_{\rm chem}}{T_{\rm chem}}, \tag{1}$$

$$\left(\frac{\eta}{s}\right)_2 = 0.2 + 0.4\,\frac{(T-T_{\rm chem})^2}{T_{\rm chem}^2}, \tag{2}$$

$$\left(\frac{\eta}{s}\right)_3 = 0.2 + 0.3\,\sqrt{\frac{T-T_{\rm chem}}{T_{\rm chem}}}. \tag{3}$$

Here $T_{\rm chem}=165$ MeV is the chemical decoupling temperature and stands for the "transition temperature" at which the hadronization of quarks and gluons is complete.

In principle, the value of η/s should exhibit a minimum near $T_{\rm chem}$ and increase again in the hadronic phase be-

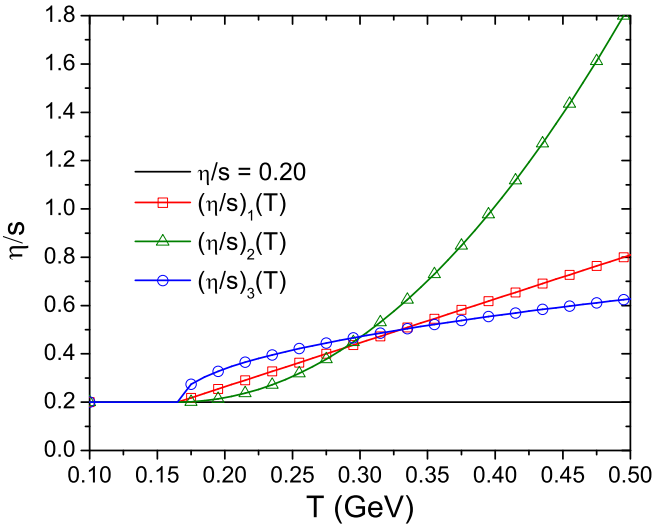


FIG. 11: (Color online) Three temperature dependent parametrizations $(\eta/s)(T)$ studied in this section. In all cases, $\eta/s = 0.2$ for $T < T_{\rm chem} = 165$ MeV.

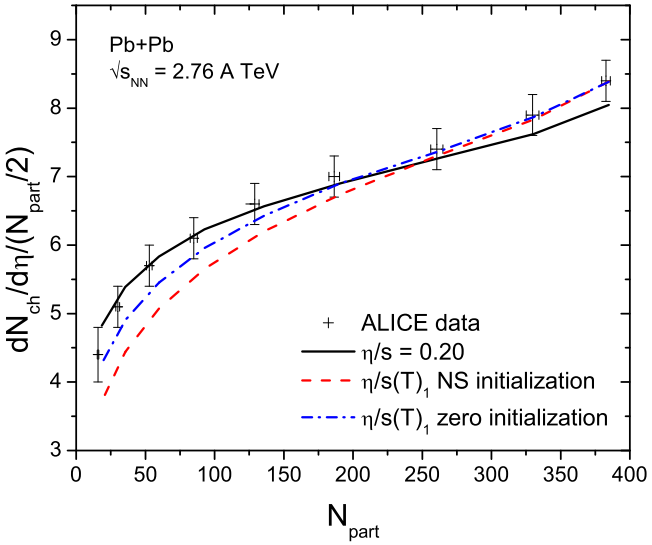


FIG. 12: (Color online) Final charged multiplicity per wounded nucleon pair as a function of number of participant nucleons in Pb+Pb collisions at $\sqrt{s} = 2.76\,A$ TeV, for different functional forms of $(\eta/s)(T)$ and initial conditions for the shear stress tensor $\pi^{\mu\nu}$ (see text).

low $T_{\rm chem}$ [58–60]. The authors of [49] pointed out, however, that at the full LHC collision energy of $5.5\,A$ TeV the behavior of η/s at temperatures below $T_{\rm chem}$ has very little effect on the final hadron spectra and their elliptic flow. At $2.76\,A$ TeV the effect on elliptic flow was moderate, and negligible on the spectra. Here we will concentrate on qualitative aspects of effects arising from a temperature dependent growths of η/s in the high temperature region that can be explored at LHC energies but is beyond the reach of RHIC, and continue to set $\eta/s = 0.2$ at $T < T_{\rm chem}$ for simplicity.

As pointed out in [49], the spectra and elliptic flow in Au+Au collisions at RHIC energies are most sensitive to the average value of η/s in the temperature region below 220-230 MeV. We have checked that altering η/s at higher temperatures as shown in Fig. 11 has little influence on the results at RHIC energies shown in Sec. II.

Figure 12 illustrates the influence of a linear temperature dependence of η/s as in Eq. (1) on the centrality dependence of charged hadron production. The solid black line is the same as shown in the upper part of Fig. 1 where it forms the lower bound of the shaded region; it corresponds to constant $\eta/s = 0.2$ and Navier-Stokes initial conditions for the shear stress tensor, $\pi^{\mu\nu} = 2\eta\sigma^{\mu\nu}$ at $\tau_0 = 0.6\,{\rm fm}/c$. The dashed and dash-dotted lines in Fig. 12 use $(\eta/s)_1(T)$ with either Navier-Stokes (dashed) or zero (dash-dotted) initial conditions for $\pi^{\mu\nu}$. These last two lines were normalized to the ALICE point for the 0−5% most central Pb+Pb collisions ($dN_{\rm ch}/d\eta = 1584 \pm 80$ [40]), whereas the black line was normalized to our best guess before the ALICE data became available ($dN_{\rm ch}/dy = 1800$, corresponding to $dN_{\rm ch}/d\eta = 1548$). The centrality dependence is then controlled by the predictions from the MC-KLN model, modified by viscous entropy production during the hydrodynamic evolution.

We see that even a relatively modest temperature dependent increase of η/s in the QGP phase leads to a significantly stronger non-linearity in the dependence of charged particle production on the number of wounded nucleons. The reason is that an increase of η/s with temperature leads to more viscous heating in central collisions (which probe higher initial temperatures and such larger effective shear viscosities) than in peripheral ones (whose initial temperatures are lower). Since the entropy production rate is given by

$$\partial_\mu S^\mu = \frac{\pi^{\mu\nu}\pi_{\mu\nu}}{2\eta T}, \qquad (4)$$

this effect is stronger for Navier-Stokes initial conditions (where $\pi^{\mu\nu}$ is proportional to the velocity shear tensor $\sigma^{\mu\nu}$ which at early times diverges like $1/\tau$) than for zero initial shear stress (where $\pi^{\mu\nu}$ starts from zero and approaches its Navier-Stokes value $2\eta\sigma^{\mu\nu}$ only after several relaxation times τ_π when, due to its $1/\tau$ decay, it has already decreased to much smaller values).[12]

If one were to postulate the validity of the MC-KLN model as the correct description of the initial particle production, the ALICE data shown in Fig. 12 would exclude

[12] For reference we list the fractions of the finally measured entropy in the most central and most peripheral centrality bins shown in Fig. 12 that are generated by viscous heating during the hydrodynamic expansion: Constant $\eta/s = 0.2$: $\Delta S/S_{\rm final} = 26\%$ (0−5%) and 33% (70−80%); $(\eta/s)_1(T)$ with $\pi_0^{\mu\nu} = 0$: $\Delta S/S_{\rm final} = 25\%$ (0−5%) and 15% (70−80%); $(\eta/s)_1(T)$ with $\pi_0^{\mu\nu} = 2\eta\sigma^{\mu\nu}$: $\Delta S/S_{\rm final} = 60\%$ (0−5%) and 49% (70−80%).

a temperature dependence of η/s as given in Eqs. (1) and (2) for Naver-Stokes initial conditions. While we are not prepared to make such a statement on the basis of Fig. 12 alone, we believe that it is important to point out this relatively strong sensitivity of the centrality dependence of $dN_{\rm ch}/d\eta$ to the transport properties of the expanding fireball medium and to emphasize the constraints it thus places on possible models for the QGP shear viscosity.

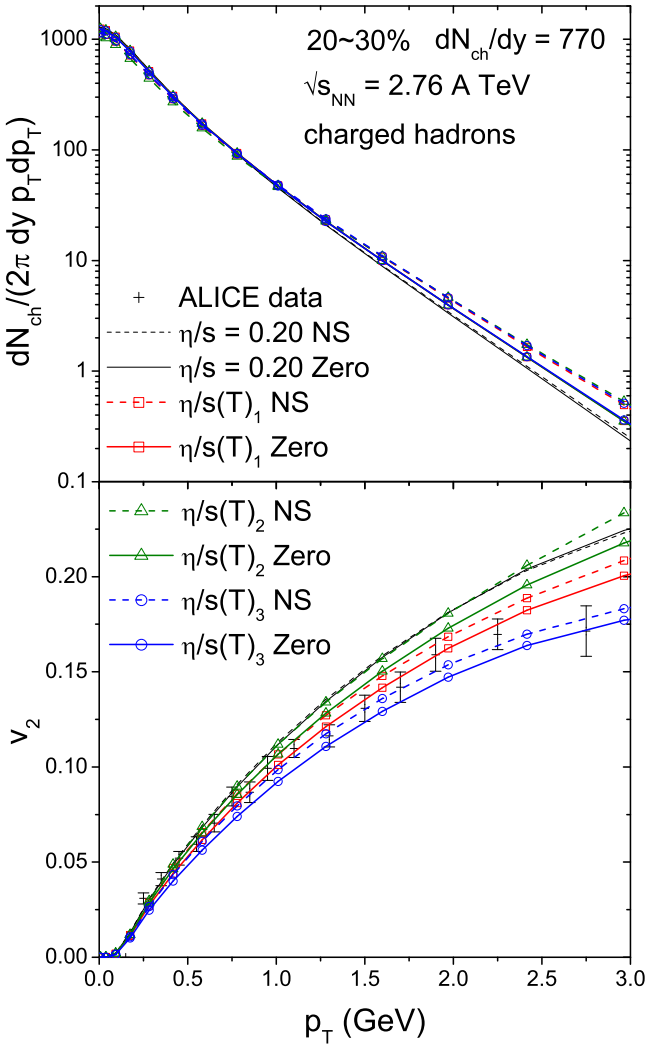


FIG. 13: (Color online) Charged hadron transverse momentum spectra (top) and differential elliptic flow (bottom) for 2.76 A TeV Pb+Pb collisions at 20−30% centrality, for different models for the temperature dependence of η/s and different initial conditions for $\pi^{\mu\nu}$ (Navier-Stokes ("NS") or 0 ("Zero")). The ALICE data in the bottom panel are from Ref. [1].

We now turn to the discussion of the influence of a possible temperature dependence of η/s on the charged hadron p_T-spectra and elliptic flow. Figure 13 shows LHC predictions for 2.76 A TeV Pb+Pb collisions of 20−30% centrality. To ensure comparability of the different cases studied in this figure we simply normalized the initial entropy density profile such that we always obtain $dN_{\rm ch}/dy = 770$, i.e. the same value that we had obtained before for constant $\eta/s = 0.2$ at this centrality. We first note that for constant $\eta/s = 0.2$, we don't observe any significant difference in the charged hadron spectra and elliptic flow between zero and Navier-Stokes initialization for $\pi^{\mu\nu}$. Turning to the temperature-dependent parametrizations $(\eta/s)_i(T)$, we note that for zero initialization of $\pi^{\mu\nu}$ (solid lines) our results agree with those reported in [49]: An increase of η/s at higher QGP temperatures leads to somewhat harder charged hadron p_T-spectra (i.e. somewhat stronger radial flow, caused by the larger tranverse effective pressure gradients at early times) and a suppression of the differential elliptic flow (due to an increase of the time-averaged effective shear viscosity of the fluid). It is interesting to observe the hierarchy of the curves in Fig. 13 corresponding to the three parametrizations (1)–(3): For the p_T-spectra, all three T-dependent viscosities lead to almost identical hardening effects on the spectral slope, while for the differential elliptic flow $v_2^{\rm ch}(p_T)$ the curves are ordered not according to the η/s-values at the initial central fireball temperature (see Table I), but according to their hierarchy in the $165 < T < 280$ MeV range. In fact, the observed magnitudes of the viscous v_2 suppression for the three $(\eta/s)(T)$ functions suggest that, at this beam energy and collision centrality, the buildup of elliptic flow is dominated by the QGP transport properties at $200 \lesssim T \lesssim 250$ MeV. (At RHIC energies, the transport properties for $T \lesssim 200-220$ MeV dominate the generation of v_2 [49].)

TABLE I: Initial central entropy densities s_0 and temperatures T_0 for the viscous hydrodynamic simulations of 20−30% centrality Pb+Pb collisions at the LHC ($\sqrt{s} = 2.76\,A$ TeV) shown in Fig. 13. The different models for the T-dependence of η/s are defined in Eqs. (1)–(3). "0" stands for $\pi_0^{\mu\nu} = 0$ at τ_0, "NS" stands for Navier-Stokes initialization of the shear stress tensor, $\pi_0^{\mu\nu} = 2\eta\sigma^{\mu\nu}$ at τ_0.

η/s model	$\pi_0^{\mu\nu}$	s_0 (fm^{-3})	T_0 (MeV)
$\eta/s = 0.2$	0	191.6	427.9
	NS	172.4	413.9
$(\eta/s)_1(T)$	0	179.6	419.2
	NS	119.3	368.7
$(\eta/s)_2(T)$	0	179.6	419.2
	NS	115.6	365.1
$(\eta/s)_3(T)$	0	175.2	416.0
	NS	116.6	366.1

For Navier-Stokes initial conditions (dashed lines in Fig. 13), the increase in radial flow caused by an increase of η/s at high temperature is stronger and the viscous v_2 suppression is weaker than for zero initial $\pi^{\mu\nu}$. This is caused by the much larger initial shear stress ten-

sor components in the NS case, compared to the case of $\pi_0^{\mu\nu}=0$ where $\pi^{\mu\nu}$ approaches its (by that time already much smaller) Navier-Stokes limit only after several relaxation times τ_π [24]. The increase of η/s with temperature generates a steeper initial transverse effective pressure gradient (since $\pi^{\mu\nu}$ grows faster than the entropy density s when η/s increases with temperature), and this generates stronger radial flow. It also causes a larger spatial eccentricity of the initial effective pressure profile which (when compared to the case of $\pi_0^{\mu\nu}=0$) generates stronger elliptic flow. In fact, we found that for earlier starting times τ_0 (where the Navier-Stokes values for $\pi^{\mu\nu}$ are even larger), the quadratic parametrization $(\eta/s)_2(T)$ with NS initial conditions can lead to *more* elliptic flow than a constant $\eta/s=0.2$, in spite of the larger mean viscosity of the fluid.

We conclude from this exercise that a firm determination whether or not the ALICE data point towards a temperature-dependent growth of η/s with increasing T, as expected from perturbative QCD [61] and (perhaps) from lattice QCD [62], is not possible without a better understanding of the initial conditions for the energy momentum tensor (in particular the shear stress components) at the beginning of the hydrodynamic evolution. Whereas generically larger viscosities cause a suppression of the elliptic flow, temperature-dependent viscosities can influence the initial effective pressure profile and its eccentricity in a way that counteracts this tendency and, for some models such as Navier-Stokes initial conditions, can even overcompensate it.

V. CONCLUSIONS

Based on an successful global fit of soft hadron production data in 200 A GeV Au+Au collisions at RHIC with a pure viscous hydrodynamic model with Cooper-Frye freeze-out, presented in Sec. II, we generated hydrodynamic predictions for the p_T-spectra and differential elliptic flow of unidentified charged hadrons and identified pions and protons for Pb+Pb collisions at the LHC. Where available, these predictions were compared with available experimental data from the ALICE Collaboration. Our extrapolation from RHIC to LHC energies was based on the assumption that the QGP shear viscosity η/s does not change with increasing fireball temperature and stays fixed at the value $\eta/s=0.2$ extracted from the RHIC data, assuming MC-KLN initial conditions. The start time τ_0 for the hydrodynamic evolution and the freeze-out temperature $T_{\rm dec}$ were held fixed, too. We found that, using the beam energy scaling implicit in the MC-KLN model, such an extrapolation gives a good description of the centrality dependence of charged hadron production and the charged hadron p_T-spectra in central Pb-Pb collisions, but overpredicts the slope of the p_T-differential elliptic flow and the value of its p_T-integrated value by about 10−15% in mid-central to mid-peripheral collisions. In the most peripheral collisions, the predicted charged hadron p_T-spectra are too flat, and the integrated elliptic flow is too small compared to the experimental data. A preliminary study of possible temperature dependent variations of η/s in the high-temperature region explored for the first time at the LHC remained unconclusive but pointed to a clear need for better theoretical control over the initial conditions for the hydrodynamic energy-momentum tensor, in particular its shear stress components. The development of detailed dynamical models for the pre-thermal evolution of the collision fireball and their matching to the viscous hydrodynamic stage is a matter of priority for continued progress towards quantifying the transport properties of the quark-gluon plasma at different temperatures and densities.

Acknowledgments

We would like to thank R. Snellings and A. Tang for providing us with tables of the experimental data from the ALICE experiment and for helpful discussions. This work was supported by the U.S. Department of Energy under contracts DE-AC02-05CH11231, DE-FG02-05ER41367, DE-SC0004286, and (within the framework of the JET Collaboration) DE-SC0004104. P.H.'s research was supported by the ExtreMe Matter Institute (EMMI) and by BMBF under contract no. 06FY9092.

[1] K. Aamodt *et al.* [ALICE Collaboration], Phys. Rev. Lett. **105**, 252302 (2010).
[2] P. Danielewicz, M. Gyulassy, Phys. Rev. D **31**, 53 (1985).
[3] U. Heinz and P. F. Kolb, Nucl. Phys. A **702**, 269 (2002).
[4] G. Policastro, D. T. Son and A. O. Starinets, Phys. Rev. Lett. **87**, 081601 (2001); P. K. Kovtun, D. T. Son and A. O. Starinets, Phys. Rev. Lett. **94**, 111601 (2005).
[5] U. Heinz and S. M. H. Wong, Phys. Rev. **C66**, 014907 (2002).
[6] D. Teaney, Phys. Rev. C **68**, 034913 (2003).
[7] I. Arsene *et al.* (BRAHMS Collaboration), Nucl. Phys. **A757**, 1 (2005); B. B. Back *et al.* (PHOBOS Collaboration), *ibid.,* p. 28; J. Adams *et al.* (STAR Collaboration), *ibid.,* p. 102; K. Adcox *et al.* (PHENIX Collaboration), *ibid.,* p. 184.
[8] R. A. Lacey and A. Taranenko, PoS **CFRNC2006**, 021 (2006); R. A. Lacey *et al.*, Phys. Rev. Lett. **98**, 092301 (2007); A. Adare *et al.*, Phys. Rev. Lett. **98**, 172301 (2007); H.-J. Drescher, A. Dumitru, C. Gombeaud, and J.-Y. Ollitrault, Phys. Rev. C **76**, 024905 (2007). K. Dusling and D. Teaney, Phys. Rev. C **77**, 034905 (2008); Z. Xu, C. Greiner, and H. Stöcker, Phys. Rev. Lett. **101**, 082302 (2008); D. Molnar and P. Huovinen, J. Phys. G **35**, 104125 (2008); R. A. Lacey, A. Tara-

nenko and R. Wei, in *Proc. 25th Winter Workshop on Nuclear Dynamics*, W. Bauer, R. Bellwied, and J.W. Harris (eds.), (EP Systema, Budapest, 2009) p. 73 [arXiv:0905.4368 [nucl-ex]]; K. Dusling, G. D. Moore, and D. Teaney, Phys. Rev. C **81**, 034907 (2010); A. K. Chaudhuri, J. Phys. G **37**, 075011 (2010); R. A. Lacey *et al.*, Phys. Rev. C **82**, 034910 (2010).

[9] P. Romatschke and U. Romatschke, Phys. Rev. Lett. **99**, 172301 (2007); M. Luzum and P. Romatschke, Phys. Rev. C **78**, 034915 (2008).

[10] H. Song, S. A. Bass, U. Heinz, T. Hirano and C. Shen, Phys. Rev. Lett. **106**, 192301 (2011); and Phys. Rev. C **83**, 054910 (2011).

[11] M. Luzum, Phys. Rev. C **83**, 044911 (2011).

[12] R. A. Lacey, A. Taranenko, N. N. Ajitanand and J. M. Alexander, Phys. Rev. C **83**, 031901 (2011).

[13] N. Armesto *et al.*, J. Phys. G **35**, 054001 (2008).

[14] H. Niemi, K. J. Eskola and P. V. Ruuskanen, Phys. Rev. C **79**, 024903 (2009)

[15] G. Kestin and U. Heinz, Eur. Phys. J. C **61**, 545 (2009); U. Heinz, Nucl. Phys. **A830**, 287c (2009).

[16] M. Luzum and P. Romatschke, Phys. Rev. Lett. **103**, 262302 (2009).

[17] P. Bozek, M. Chojnacki, W. Florkowski and B. Tomasik, Phys. Lett. **B694**, 238 (2010); P. Bozek, *ibid.* **B699**, 283 (2011).

[18] T. Hirano, P. Huovinen and Y. Nara, Phys. Rev. C **83**, 021902 (2011).

[19] B. Schenke, S. Jeon and C. Gale, Phys. Lett. **B702**, 59 (2011).

[20] H. Song, S. A. Bass and U. Heinz, Phys. Rev. C **83**, 054912 (2011).

[21] T. Hirano, U. Heinz, D. Kharzeev, R. Lacey and Y. Nara, Phys. Lett. **B636**, 299 (2006).

[22] H. Song, S. A. Bass and U. Heinz, Phys. Rev. C **83**, 024912 (2011).

[23] T. Hirano, U. Heinz, D. Kharzeev, R. Lacey and Y. Nara, J. Phys. G **34**, S879 (2007).

[24] H. Song and U. Heinz, Phys. Lett. **B658**, 279 (2008); Phys. Rev. C **77**, 064901 (2008); **78**, 024902 (2008); H. Song, Ph.D Thesis, The Ohio State University (August 2009) [arXiv:0908.3656 [nucl-th]].

[25] P. Huovinen and P. Petreczky, Nucl. Phys. **A837**, 26 (2010).

[26] C. Shen, U. Heinz, P. Huovinen and H. Song, Phys. Rev. C **82**, 054904 (2010).

[27] F. Cooper and G. Frye, Phys. Rev. D **10**, 186 (1974).

[28] J. Sollfrank, P. Koch and U. Heinz, Phys. Lett. **B252**, 256 (1990); Z. Phys. C **52**, 593 (1991); J. Sollfrank, P. Huovinen, M. Kataja, P. V. Ruuskanen, M. Prakash and R. Venugopalan, Phys. Rev. C **55**, 392 (1997).

[29] A. Adil, H. J. Drescher, A. Dumitru, A. Hayashigaki and Y. Nara, Phys. Rev. C **74**, 044905 (2006).

[30] H. J. Drescher and Y. Nara, Phys. Rev. C **76**, 041903 (2007).

[31] D. Kharzeev, M. Nardi, Phys. Lett. **B507**, 121 (2001); D. Kharzeev, E. Levin, Phys. Lett. **B523**, 79 (2001).

[32] T. Hirano and Y. Nara, Phys. Rev. C **79**, 064904 (2009); and Nucl. Phys. **A830**, 191C (2009).

[33] Z. Qiu and U. Heinz, Phys. Rev. C **84**, 024911 (2011).

[34] B. B. Back *et al.* [PHOBOS Collaboration], Phys. Rev. C **70**, 021902 (2004); B. Alver *et al.* [PHOBOS Collaboration], *ibid.* **80**, 011901 (2009).

[35] J. L. Albacete and A. Dumitru, arXiv:1011.5161 [hep-ph].

[36] I. Balitsky, Phys. Rev. D **75**, 014001 (2007).

[37] J. L. Albacete, Phys. Rev. Lett. **99**, 262301 (2007).

[38] Y. V. Kovchegov and H. Weigert, Nucl. Phys. **A784**, 188 (2007); Nucl. Phys. **A807**, 158 (2008).

[39] K. Aamodt *et al.* [ALICE Collaboration], Phys. Rev. Lett. **106**, 032301 (2011).

[40] K. Aamodt *et al.* [ALICE Collaboration], Phys. Rev. Lett. **105**, 252301 (2010).

[41] J. Adams *et al.* [STAR Collaboration], Phys. Rev. Lett. **91**, 172302 (2003).

[42] S. S. Adler *et al.* [PHENIX Collaboration], Phys. Rev. C **69**, 034910 (2004).

[43] J. Adams *et al.* [STAR Collaboration], Phys. Rev. Lett. **92**, 112301 (2004); B. I. Abelev *et al.* [STAR Collaboration], *ibid.* **97**, 152301 (2006).

[44] B. I. Abelev *et al.* [STAR Collaboration], Phys. Rev. C **79**, 034909 (2009).

[45] S. S. Adler *et al.* [PHENIX Collaboration], Phys. Rev. C **69**, 034909 (2004).

[46] Y. Bai, Ph.D. Thesis, NIKHEF and Utrecht University, The Netherlands (2007).

[47] B. I. Abelev *et al.* [STAR Collaboration], Phys. Rev. C **77**, 054901 (2008).

[48] C. Shen and U. Heinz, Phys. Rev. C **83**, 044909 (2011).

[49] H. Niemi, G. S. Denicol, P. Huovinen, E. Molnar and D. H. Rischke, Phys. Rev. Lett. **106**, 212302 (2011).

[50] K. Aamodt *et al.* [ALICE Collaboration], Phys. Lett. **B696**, 30 (2011).

[51] K. Aamodt *et al.* [ALICE Collaboration], Phys. Rev. Lett. **107**, 032301 (2011); R. Snellings *et al.* [ALICE Collaboration], arXiv:1106.6284 [nucl-ex].

[52] J. Y. Ollitrault, A. M. Poskanzer and S. A. Voloshin, Phys. Rev. C **80**, 014904 (2009).

[53] P. F. Kolb and U. Heinz, in *Quark-Gluon Plasma 3*, edited by R. C. Hwa and X.-N. Wang (World Scientific, Singapore, 2004), p. 634 [arXiv:nucl-th/0305084];

[54] J. Adams *et al.* [STAR Collaboration], Phys. Rev. C **72**, 014904 (2005).

[55] C. Shen, B. Schenke, and U. Heinz, in preparation.

[56] A. Monnai and T. Hirano, arXiv:1102.5053 [nucl-th].

[57] T. Hirano and K. Tsuda, Phys. Rev. C **66**, 054905 (2002).

[58] L. P. Csernai, J. I. Kapusta and L. D. McLerran, Phys. Rev. Lett. **97**, 152303 (2006)

[59] J. W. Chen, M. Huang, Y. H. Li, E. Nakano and D. L. Yang, Phys. Lett. **B670**, 18 (2008).

[60] J. I. Kapusta, in *Relativistic Heavy Ion Physics*, Landolt-Börnstein New Series, Vol. I/23, edited by R. Stock, (Springer Verlag, New York, 2010) [arXiv:0809.3746 [nucl-th]].

[61] P. B. Arnold, G. D. Moore and L. G. Yaffe, JHEP **0305**, 051 (2003).

[62] H. B. Meyer, Phys. Rev. D **76**, 101701 (2007).